Novel probe of graviton dispersion relations at nanohertz frequencies

Bill Atkins[,1,*] Ameek Malhotra[,1,†] and Gianmassimo Tasinato[1,2,‡]

[1]*Physics Department, Swansea University, Swansea SA2 8PP, United Kingdom*
[2]*Dipartimento di Fisica e Astronomia, Università di Bologna, INFN, Sezione di Bologna,*
I.S. FLAG, viale Berti Pichat 6/2, 40127 Bologna, Italy

We generalize Phinney's "practical theorem" to account for modified graviton dispersion relations motivated by certain cosmological scenarios. Focusing on specific examples, we show how such modifications can induce characteristic localized distortions—bumps—in the frequency profile of the stochastic gravitational wave background emitted from distant binary sources. We concentrate on gravitational waves at nanohertz frequencies probed by pulsar timing arrays, and we forecast the capabilities of future experiments to accurately probe parameters controlling modified dispersion relations. Our predictions are based on properties of gravitational waves emitted in the first inspiral phase of the binary process and do not rely on assumptions of nonlinear effects occurring during the binary merging phase.

I. INTRODUCTION

The physics of gravitational waves (GWs) offers new perspectives for testing our understanding of a multitude of physical phenomena and their theoretical interpretations—including providing insights into gravitational interactions, cosmology, and astrophysics (see, e.g., [1,2] for a pedagogical treatment of these subjects). In this work, we discuss a novel approach for probing the GW dispersion relations based on a generalization of Phinney's practical theorem [3] to allow for GW dispersion relations different than the case predicted by general relativity. We use propagation effects of GWs traveling cosmological distances. We remain (for the most part) agnostic to the source of the dispersion relations, but take inspiration by applying this to the case of modified gravity.

The multimessenger event GW170817 [4–6] set very stringent bounds on any deviations of the speed of gravity c_T from the speed of light c_γ: $|c_T - c_\gamma| \leq 3 \times 10^{-15}$. This result ruled out many dark energy models based on non-minimal couplings of extra degrees of freedom with gravity, as shown in [7–10], building also on ideas explored in [11–14] (henceforth, we choose units where the speed of light $c_\gamma = 1$). However, it is important to note the GW170817 constraint holds at the hertz frequencies characteristic of LIGO-Virgo-KAGRA (LVK) detections, and it is possible that at different scales one finds $c_T \neq 1$, due to frequency-dependent modifications of the graviton dispersion relations. In fact, modified gravity models of dark energy in the Horndeski class (see, e.g., [15] for a review) or vector-tensor theories (see, e.g., [16]) predict a $c_T \neq 1$ at low energies around spontaneously Lorentz-breaking backgrounds, caused by derivative interactions with the metric.[1] Their Lorentz invariant ultraviolet completions, if they exist, should recover a GW luminal speed at high frequencies [20], in particular, in the LVK band suggesting that the dispersion relations may not yet be directly observable by experimentation. Concrete studies based on applications of advanced effective field theory techniques to dark energy setups, for example [21], suggest that a departure from the $c_T = 1$ relation should be expected. Moreover, given our ignorance of the real nature of dark matter and dark energy, it is important to keep an open mind over scenarios able to efficiently scatter GWs traveling over the cosmic medium (as, for example, solid dark matter [22,23]). Such scenarios motivate modified GW dispersion relations, a topic well explored in the past decades (see, e.g., [24–27]).

At the present stage, in addition to the theoretical aspects of the subject—currently under interesting development—it is also important to exploit forthcoming experimental opportunities and explore phenomenological ways to test modifications of standard GW propagation at different frequencies with GW experiments. In particular, the aforementioned scenarios might predict rapid changes in the

---

*Contact author: bill.atkins847@gmail.com
†Contact author: ameek.malhotra@swansea.ac.uk
‡Contact author: g.tasinato2208@gmail.com

---

[1]Possible exceptions can be realized in degenerate higher order scalar-tensor scenarios [17–19].

values of c_T as a function of frequency (see, e.g., [20]) which motivate the search for methods to test them. From the point of view of observations, apart from the 10-Hz range of LVK measurements, there are existing or prospective bounds on $|c_T - c_\gamma|$ at different frequency scales. At GW frequencies $10^{-18} \le f/\mathrm{Hz} \le 10^{-14}$ there are constraints from the cosmic microwave background [28]. At frequencies $f/\mathrm{Hz} \simeq 10^{-5}$ there are Hulse-Taylor-type bounds [29]. For the $10^{-4} \le f/\mathrm{Hz} \simeq 10^{-2}$ range, we will be able to use the redshift induced waveform dependence [30] for Laser Interferometer Space Antenna (LISA) [31], as well as its frequency dependence [32]. For $10^{-4} \le f/\mathrm{Hz} \simeq 10^3$, there are ideas based on multiband detections [32,33]. Also the ringing properties of perturbations of black hole horizons can, in principle, be used to set constraints on c_T, see, e.g., [34,35].

The list above does not include nanohertz frequencies, which are interesting to investigate given the new possibilities offered by strong hints of detection of a stochastic gravitational wave background (SGWB) [36–39] at those frequency scales [see Ref. [40] for a study within the NANOGrav Collaboration to detect new physics with recent pulsar timing array (PTA) data]. Recent studies explore modifications of PTA response functions [41–44] that occur when $c_T \ne 1$, while various works (see, e.g., [45–50]) study further consequences of modified gravity on PTA data. Here, instead, we consider a novel effect—a distortion in the frequency profile of a SGWB produced by supermassive black hole (SMBH) binaries, which is induced by a frequency-dependent change in the value of c_T at around the nanohertz scales. This effect exploits propagation effects when GW dispersion relations are modified and, if detected, would allow us to experimentally probe a frequency-dependent c_T with PTA experiments. In particular, it allows us to measure the case of a c_T varying with frequency, a phenomenon that would be difficult to analyze with the alternative methods devised so far. Moreover, as an important by-product, it can also provide independent information about the redshift distribution of the sources of SGWB.

To develop our understanding of the physics we wish to explore, we generalize Phinney's theorem [3] to show that the aforementioned frequency-dependent value of c_T modifies the frequency profile of the SGWB spectrum—as discussed in Sec. II. This effect leads to a deformation (a "bump,") on an otherwise power-law GW spectrum profile. The properties of the bump depend both on the frequency dependence of c_T and on the redshift of the SMBH sources. Interestingly, the aforementioned implications of modified dispersion relations take place during GW emission occurring in the very first inspiral phase of the SMBH merging process, at zeroth order in a post-Newtonian approximation. Hence, it is not influenced by screening effects (Vainshtein mechanism, etc.) that characterize many modified gravity models and that, due to nonlinearities, make a

comparison with observations particularly difficult—see, e.g., [15] for a review. In Sec. III, building on [51,52], we perform Fisher forecasts on the prospects of future PTA observations to set bounds on c_T when monitoring a large number of pulsars, examining how the result depends on the modified dispersion relations and on the source properties. We conclude in Sec. IV. We set $c_\gamma = G_N = 1$.

II. A GENERALIZATION OF PHINNEY'S THEOREM

Phinney's theorem relates the energy density in GWs with an integral in frequency and redshift of quantities associated with GW sources and GW propagation. In fact, in their propagation from source to detection, GWs can experience modified gravity effects that change the standard relation between GW frequency at emission and detection. Precisely such cosmological "redshift" effects, which are well studied in the different context of modifications of GW luminosity distance (see, e.g., [53,54]), are at the basis of our generalization of Phinney's theorem in a modified gravity setting.

To start with, let us develop some basic formulas relating GW frequencies at emission and detection. We assume that the GW speed c_T depends on the GW momentum, and we restrict the gravitational wave speed to be subluminal, with a dispersion relation taking the form of

$$\omega(\mathbf{k}) = c_T(\mathbf{k})\mathbf{k}, \qquad \mathbf{k} = |\vec{k}|, \qquad c_T(\mathbf{k}) \le 1. \quad (2.1)$$

To be precise, we must distinguish between the gravitational wave phase velocity, $v_{ph} = \omega(\mathbf{k})/\mathbf{k}$ and the group velocity $v_{gr} = \partial\omega/\partial\mathbf{k}$. As we wish to remain agnostic to the source of the dispersion relations and model using a simple wave packet, we presently restrict our analysis to only considering the phase velocity, whereby a complete analysis of the phase and group velocities depends on one's choice of $c_T(\mathbf{k})$ ansatz (further discussion may be found in [42,55]). See Sec. I for the theoretical motivations supporting this possibility. Now proceeding along the lines of the arguments developed in [30,56] (building on [1]), we can write the comoving distance covered by GWs along their way to detection as

$$r_{\mathrm{com}}^{(\mathrm{GW})}(t) = \int_0^r d\tilde{r} = \int_{t_e}^t d\tilde{t}\, \frac{c_T[f(\tilde{t})]}{a(\tilde{t})}, \quad (2.2)$$

where we notice that the comoving distance depends on the frequency-dependent GW speed $c_T(f)$. From now on, we interchange the momentum-dependent $c_T(\mathbf{k})$ with a frequency-dependent $c_T(f)$, making use of the implicit relation $k = 2\pi f/c_T(f)$ between frequency and momentum. Let us now consider two wave crests crossing the same comoving distance, following relation (2.2). The difference between the times of detection is related to the difference

among time of emission of the wave crests, by (the suffix d indicates detection position, while s is the source position)

$$\Delta t_d = \frac{a(t_d)}{a(t_s)} \frac{c_T[f(t_s)]}{c_T[f(t_d)]} \Delta t_s. \tag{2.3}$$

This implies that the GW frequencies, proportional to the inverse of the wave crest Δt's, satisfy

$$f_s = \frac{(1+z)}{1-\Delta} f_d, \tag{2.4}$$

with Δ given by

$$\Delta = 1 - \frac{c_T(f_d)}{c_T(f_s)}. \tag{2.5}$$

The quantity Δ controls the frequency-dependent GW speed and plays an essential role in our arguments. It depends on the GW speed c_T at frequencies measured at the position of the source and of detection. Differentiating Eq. (2.4), we find

$$\frac{df_s}{f_s} = \frac{df_d}{f_d}\left(1 - \frac{d\ln(1-\Delta)}{d\ln(f_d)}\right). \tag{2.6}$$

These formulas are at the basis of our generalization of Phinney's theorem: we follow [3], instead using (2.4) to relate frequencies at different redshifts. The total present-day energy density in GWs, as detected by GW experiments, can be expressed as

$$\mathcal{E}_{\mathrm{GW}} = \int_0^\infty \rho_c\,\Omega_{\mathrm{GW}}(f_d)\frac{df_d}{f_d}, \tag{2.7}$$

with Ω_{GW} the GW energy density for logarithmic frequency interval, divided by the critical density ρ_c. On the other hand, the quantity $\mathcal{E}_{\mathrm{GW}}$ is a sum of energy densities as radiated at each redshift, taking into account the differential relation

$$d\mathcal{E}_{\mathrm{GW}}^{(d)} = \frac{1-\Delta}{1+z}d\mathcal{E}_{\mathrm{GW}}^{(s)}. \tag{2.8}$$

Integrating, we find

$$\begin{aligned}\mathcal{E}_{\mathrm{GW}} = \int_0^\infty \int_0^\infty &\frac{N(z)}{1+z}\left[1-\Delta-\frac{d(1-\Delta)}{d\ln(f_d)}\right]\\ &\times\left(f_s\frac{d\mathcal{E}_{\mathrm{GW}}^{(s)}}{df_s}\right)\frac{df_d}{f_d}dz,\end{aligned} \tag{2.9}$$

where $N(z)$ is the number of events for unit comoving volume, occurring between z and $z+dz$. Then, equating relations (2.7) and (2.9), we obtain

$$\begin{aligned}\rho_c\Omega_{\mathrm{GW}}(f_d) = \int_0^\infty &dz\frac{N(z)}{1+z}\left[1-\Delta-\frac{d(1-\Delta)}{d\ln(f_d)}\right]\\ &\times\left(f_s\frac{d\mathcal{E}_{\mathrm{GW}}^{(s)}}{df_s}\right)_{f_s=\frac{(1+z)}{(1-\Delta)}f_d},\end{aligned} \tag{2.10}$$

which represents our generalization of Phinney's theorem. The generalization includes the quantity between parentheses in Eq. (2.10), as well as the evaluation of quantity at the frequency source $f_s = (1+z)f_d/(1-\Delta)$, which includes the effects of Δ as given in Eq. (2.5).

Before proceeding, let us make a concrete toy example to explore what we can expect from the previous formula. Let us assume all sources emit at a common redshift z_0 and consist of binaries in circular orbits. At the leading (zeroth order) post-Newtonian expansion, the emitted GW energy reads (see, e.g., the textbook [1])

$$f_s\frac{d\mathcal{E}_{\mathrm{GW}}^{(s)}}{df_s} = f_s\frac{\pi}{3}\frac{\mathcal{M}^{5/3}}{(\pi f_s)^{1/3}}, \tag{2.11}$$

with $\mathcal{M} = (M_1 M_2)^{3/5}(M_1+M_2)^{-1/5}$ being the binary chirp mass. This is the GW energy density emitted during the initial, inspiral phase of the merging event. We assume that this formula is valid also in a modified gravity setup, being derived in a Newtonian approximation. Plugging into Eq. (2.10) and making use of Eq. (2.4), we find

$$\Omega_{\mathrm{GW}}(f_d) = \frac{8(\pi\mathcal{M})^{5/3}}{9H_0^2}f_d^{2/3}\frac{N(z_0)}{(1+z_0)^{1/3}}\left[\frac{\left(1-\frac{d\ln(1-\Delta)}{d\ln f_d}\right)}{(1-\Delta)^{1/3}}\right]. \tag{2.12}$$

We recognize the characteristic, well-known $f^{2/3}$ power-law profile of the GW energy density, although weighted by the quantity between square brackets, which depends on the modified GW dispersion relations associated with the quantity Δ of Eq. (2.5). If measured, this effect also provides information on the frequency dependence profile of c_T, a feature that is difficult to extract by other means. The argument of the square brackets in Eq. (2.12) is the frequency f_d at the detector, which depends on the redshift z of the source [see Eq. (2.4)]; hence the new part in the square brackets depends *both* on frequency and redshift. Such modified gravity effects, if detected, can then be used as cosmic ladders and provide independent information on the source redshift. To deduce this result, we do not have to make any assumption on strong gravity effects, nor on the behavior of screening mechanisms in specific modified gravity scenarios during the nonlinear binary merging process.

While the above formula is obtained for sources at fixed redshift, it can easily be generalized (at least formally) to a population of GW sources at different redshifts. We can write the GW energy density as

$$\Omega_{\text{GW}}(f_d) = \frac{8(\pi\mathcal{M})^{5/3}}{9H_0^2} f_d^{2/3} K \mathcal{N}_0, \qquad (2.13)$$

with $\mathcal{N}_0 = \int dz N(z)$ and

$$K = \frac{1}{\mathcal{N}_0} \int dz \frac{1}{(1-\Delta(f_d,z))^{1/3}}$$
$$\times \left(1 - \frac{d\ln(1-\Delta(f_d,z))}{d\ln f_d}\right) \frac{N(z)}{(1+z)^{1/3}}. \qquad (2.14)$$

Details on the source population as a function of redshift affects the factor K in Eq. (2.13), which depends on the modifications in the GW dispersion relations through the quantity Δ. Hence, if detected, the effects of modified gravity can also probe the redshift distribution of the GW source population.

We proceed by refining and applying the formulas obtained above to concrete settings. For the remainder of this section, for simplicity, we focus on sources emitting at a specific redshift z_0. (In the next section, we will go beyond this approximation.) We make a phenomenological
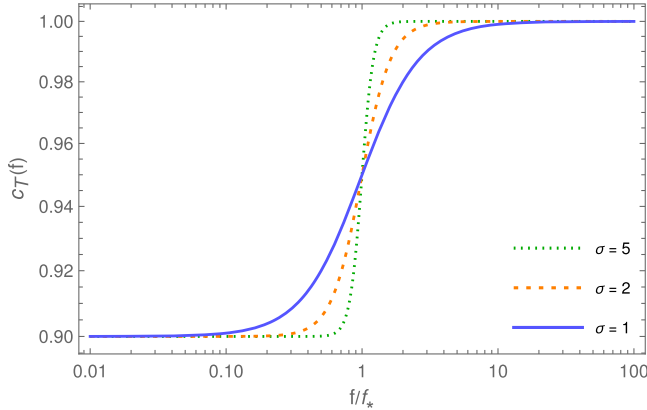

FIG. 1. The quantity c_T as a function of f/f_* for $\sigma = 1, 2, 5$, demonstrating the behavior of the ansatz (2.15) for $c_0 = 0.9$.

assumption on the behavior of c_T as a function of frequency. We choose to use the model established in [32], namely,

$$c_T(f,\sigma,f_*) = c_0 + (1-c_0)\left(\frac{1}{2} + \frac{1}{2}\tanh\left[\sigma\ln\left(\frac{f}{f_*}\right)\right]\right). \qquad (2.15)$$

Schematically, this ansatz for c_T generates a transition at a reference frequency f_*, from c_0 to 1, such that $c_T = 1$ at the frequencies detectable by Earth-based interferometers. If $f_\star$ is sufficiently far from the frequency band of LVK detections (around 10 Hz), the stringent GW170817 bounds are readily satisfied. This choice of dispersion model is not exhaustive, and it is (in part) designed to describe the modified gravity scenarios proposed in [20]. One may also perform the following analysis for several different models with differing frequency-dependent patterns for c_T, as discussed, e.g., in [30]. However, our choice of ansatz is particularly easy to manipulate, relying only on three parameters: σ, controlling the "steepness" of the transition from c_0 to c_γ; f_* controlling the position of the transition; and c_0 being the limit of c_T at low frequencies as shown in Fig. 1.

Further to this, one may easily expand upon this ansatz by introducing additional parameters to precisely describe the nature of the transition or the nature of c_T in the asymptotics. For this work, it is sufficient to consider the simplest case, whereby no additional parameters are included. Taking $\sigma = 1$ and placing Eq. (2.15) into Eq. (2.5) yields

$$\Delta(f_d,f_s,c_0,f_*) = \frac{c_0 f_*^2(1-c_0)(f_d-f_s)(2c_0 f_*+f_d+f_s)}{(f_d^2+2c_0 f_d f_*+c_0 f_*^2)(c_0 f_*+f_s)^2}. \qquad (2.16)$$

Subsequently, placing Eq. (2.16) into Eq. (2.12) provides our result for the GW energy density in the simplest example of sources emitting at the same redshift z_0, as in the toy example of Eq. (2.12). We find $\Omega_{\text{GW}}(f/f_*, c_0, z_0)$ produces a deviation from the typical $f^{2/3}$ scaling around the
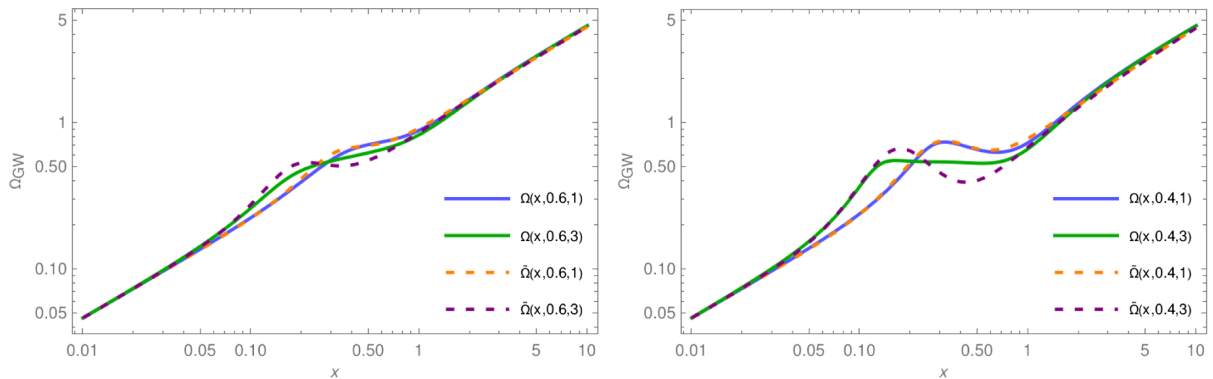

FIG. 2. Plot of the quantity $\Omega_{\text{GW}}(x, c_0, z_0)$ (with $x = f/f_*$) for $z_0 = 1, 3$ with $c_0 = 0.6, 0.4$ (respectively, left and right panels). We also examine the quality of fit of the model in Eq. (2.17).

characteristic frequency f_* characterizing ansatz (2.15), with the magnitude and placement of the deviation dependent on the choice of z_0 and c_0. The distorted SGWB frequency profile acquires a characteristic localized bump (see Fig. 2) which may make it distinguishable from other effects such as orbital eccentricities or post-Newtonian corrections. We emphasize that this bump depends on the frequency dependence of c_T, which can be captured by the modified gravity effects we are presenting here.

Increasing the strength of the dispersion (decreasing c_0) results in a more sizable localized distortion from the $f^{2/3}$ profile, which is magnified at larger redshift, where the magnitude and position of the deviation increases dramatically. We construct a numerical fit for the frequency profile of Ω_{GW}, in terms of a combination of Padé approximants to reduce the full expression of Ω_{GW} to a manageable form. The fit is chosen to asymptote to $f^{2/3}$, with deviations depending on the parameters c_0 characterizing our ansatz (2.15) and the source redshift z_0. It reads, defining $x = f/f_*$ and omitting for simplicity a constant normalization factor (which will be included later),

$$\tilde{\Omega}_{GW}(x, c_0, z_0) = x^{\frac{2}{3}}\left[1 + \frac{30(1-c_0^{\frac{1}{3}})x^3\sqrt{z_0}\left(\frac{3}{\sqrt{1+c_0+\frac{5-5\sqrt{z_0}}{5+z_0}}} - c_0\right)^3\left(1.7 + 1.5c_0x - \frac{4.5x}{\sqrt{1+c_0+\frac{5-5\sqrt{z_0}}{5+z_0}}}\right)}{1 + 30c_0x^5\left(\frac{3}{\sqrt{1+c_0+\frac{5-5\sqrt{z_0}}{5+z_0}}} - c_0\right)^5}\right]. \qquad (2.17)$$

The previous function reduces to the usual $x^{2/3} \propto f^{2/3}$ profile when $c_0 = 1$. Notice that deviations from the usual profile depend both on c_0 and z_0, hence they can be sensitive to redshift. If modified gravity is measured using this method, its effects can be used as a distance ladder. To assess the quality of fit, we plot in Fig. 2 a comparison of the fit model and the original Ω_{GW} with differing choices of c_0. Figure 2 demonstrates a close correspondence between Ω_{GW} and the fit in Eq. (2.17) at $z_0 \leq 2$ and $c_0 \geq 0.3$. It also shows that, as z_0 increases, the model begins to diverge from the numerical Ω_{GW}. For the purposes of this study, we may comfortably restrict to lower z, as numerical simulations [57] and experimental results [58] show that the peak of the contribution (from astrophysical sources) to the stochastic gravitational wave background is associated with redshifts $z \leq 1$.

Following this theoretical section in which we developed formulas generalizing Phinney's theorem to modified gravity setup at fixed redshift, we proceed to apply our results to forecast the ability of future pulsar timing array experiments to detect distortions of the frequency of Ω_{GW} and further include the redshift dependence of the sources themselves.

III. FISHER FORECASTS

In the previous section, we pointed out that a frequency-dependent GW speed $c_T(f)$ modifies the predictions of Phinney's theorem. The effect is associated with propagation properties of GWs from source to detection. This effect consequently causes a localized distortion—a bump—on the $f^{2/3}$ frequency profile characterizing the SGWB emitted by binaries in circular orbits, see Fig. 2. In this section, we investigate whether future experiments can be sensitive to the quantity c_0 of Eq. (2.15) characterizing the deviation of c_T from luminal speed at small frequencies. We also wish to understand whether modified gravity effects, if present, can inform us about the nature of the GW source (redshift, population properties, etc.). Making use of the Fisher formalism (see, e.g., [59]), we forecast the detectability of such effects with future PTA observations. Given the recent strong hint of detection of a SGWB with PTA [36–39], this topic is very timely. We assume from now on that the SGWB detected by PTA measurements is sourced by SMBH binaries in a merging process. We separate the discussion into two parts, depending on our hypothesis on the distribution of signal sources.

So far, PTA measurements are unable to precisely measure the details of the slope of the SGWB frequency profile. In the future, measuring more pulsars and/or reducing the corresponding noise sources, the situation should improve. To address this topic, we adopt an approach motivated by [51,52], and we consider an idealized situation of N_{psr} monitored pulsars (with N_{psr} a large number) isotropically located in the sky, all with the same noise properties. This is certainly an idealized situation, but in first approximation it mimics what we can achieve in the forthcoming Square Kilometre Array era [60,61], when we will be able to monitor hundreds of millisecond pulsars.

Instead of Ω_{GW}, we focus on the GW intensity $\mathcal{I}$ as a quantity more commonly studied in PTA data analysis. We assume the fit $\tilde{\Omega}_{GW}$ in Eq. (2.17) as a theoretical template for the GW energy density, including the effects of modified GW dispersion relations. The GW intensity then reads

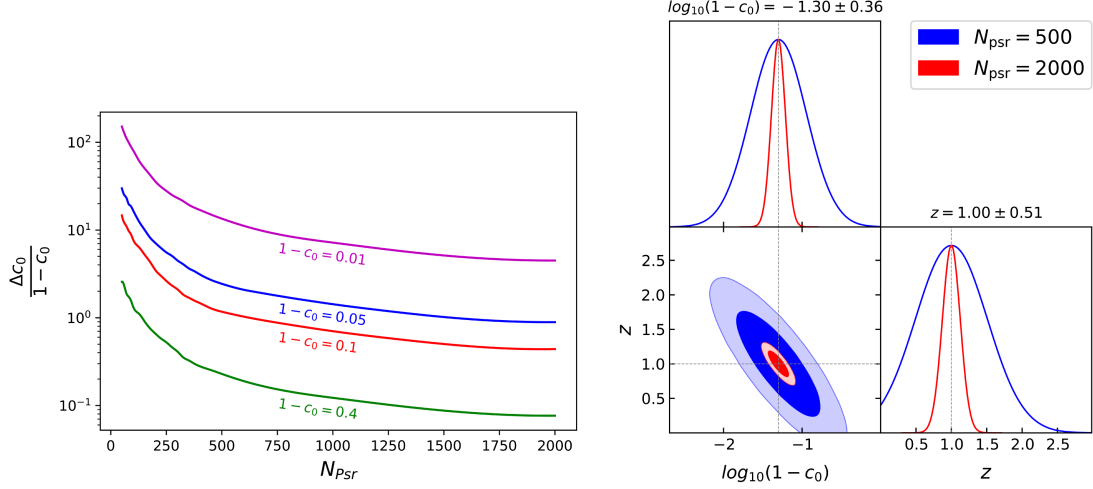$$\mathcal{I} = \frac{3H_0^2}{4\pi^2 f^3}\Omega_0\tilde{\Omega}_{GW}, \qquad (3.1)$$

FIG. 3.   Left: the relative error in c_0 as a function of N_{psr} for $1 - c_0 = 10^{-1}$ to $1 - c_0 = 10^{-2}$ marginalized over redshift. Right: the relative error ellipses for $\log_{10}(1 - c_0)$ against z for $N_{\mathrm{psr}} = 500, 2000$ and $1 - c_0 = 5 \times 10^{-2}$ with all sources located at the benchmark value $z = 1$. The quoted errors refer to the $N_{\mathrm{psr}} = 500$ case.

where the overall constant factor Ω_0 captures the overall normalization omitted in the fitting template (2.17) for the SGWB frequency profile. In measuring the intensity of the GW, we can learn about the amplitude and frequency dependence of the SGWB, but also set constraints on the quantities c_0 and z characterizing the theoretical fit $\tilde{\Omega}_{\mathrm{GW}}$ of Eq. (2.17). These are, in fact, the quantities we are interested in and seek to constrain with future datasets. From now on, we set $\Omega_0 = 8.1 \times 10^{-9}$ (such that the spectrum aligns with the amplitude measured by NANOGrav in [36]), and we choose a reference frequency $f_* = 1 \times 10^{-8}$ (to be in line with the order of magnitude of the typical frequencies used for PTA experiments).

A. Sources at common redshift z

To start our analysis, we make the initial simplification by assuming all SMBH sources occur at a fixed redshift z. PTA experiments measure time delays on millisecond pulsar periods. To detect GWs, we correlate measurements between pulsar pairs, each pulsar in the pair denoted with (a, b). Correspondingly, we build a Gaussian log-likelihood in terms of the GW intensity, evaluated at a fixed frequency f within a band Δf,

$$\mathcal{L}_f = -\log(L) = \frac{1}{2}(d - \mu)C^{-1}(d - \mu)^T, \quad (3.2)$$

where d corresponds to the vector of measured data, C_{ij} is the covariance matrix, and μ represents the vector of length $N_{\mathrm{pair}} = N_{\mathrm{psr}}(N_{\mathrm{psr}} - 1)/2$, containing the cross-power spectrum of the gravitational wave induced time residuals for distinct pulsar pair. We denote the latter with $\mathcal{R}_{ab}^{\mathrm{GW}}$. To be

explicit, each element of μ contains $\mathcal{R}_{ab}^{\mathrm{GW}}$ plus noise, however, as we shall soon search for the expectation values of $\mathcal{R}_{ab}$, we anticipate the noise contributions average to zero (more on this later). We assume that the intensity $\mathcal{I}$ is isotropic and independent from the GW direction. The quantity $\mathcal{R}_{ab}^{\mathrm{GW}}$, at a given frequency, results

$$\mathcal{R}_{ab}^{\mathrm{GW}} = \frac{\mathcal{I} \cdot \mathcal{H}(\nu)}{(4\pi f)^2}, \quad (3.3)$$

with $\nu = \hat{a} \cdot \hat{b}$ being the angle between the pulsar directions (with respect to Earth) in a given pulsar pair. We take for the function $\mathcal{H}(\nu)$ the Hellings-Downs formula [62]

$$\mathcal{H}(\nu) = \frac{3 + \nu}{3} + 2(1 - \nu) \ln\left(\frac{1 - \nu}{2}\right). \quad (3.4)$$

In fact, we might expect corrections to this formula for modified dispersion relations, which have been computed in the limit of frequency-independent, constant c_T (see, e.g., [41–44]). However, we take the Hellings-Downs result as first approximation in our setup where c_T has a pronounced frequency dependence in the PTA band. If the induced effects from modified gravity corrections are small, this remains a reasonable first order approximation; however, it is also important to note that if corrections are prominent at characteristic frequencies, they may help break the degeneracies similarly to those seen in Fig. 3. We now proceed to label each pair of distinct pulsars with capital indices, $I = (a, b)$, as in [51]. As mentioned above, we make the hypothesis that all pulsars have identical noise properties. We assume a weak-signal limit

where the background signal is subdominant to the intrinsic common pulsar noise, which we define as σ_p; namely,[2]

$$\mathcal{I} \ll (4\pi f)^2 \sigma_p^2. \qquad (3.5)$$

We select for our analysis a time of observation

$$T_{\rm obs} = 15 \text{ yr}, \qquad (3.6)$$

as in the current NANOGrav dataset. We are then able to work with a diagonal covariance matrix of the form [51]

$$C_{IJ} \approx \frac{\sigma_a^2 \sigma_b^2}{2 T_{\rm obs} \Delta f}. \qquad (3.7)$$

We then generate our noise curve from the HASASIA package [63] with $N_{\rm psr}$ uniformly generated pulsars, choosing (for the white noise parameters) a cadence $T_{\rm cad} = {\rm yr}/15$, and selecting $\Delta t_{\rm rms} = 100$ ns to be the rms error of the timing residuals. For the red noise parameters, we select $A_{\rm RN} = 2 \times 10^{-15}$, and $\alpha_{\rm RN} = -2/3$ in line with [64] such that we remain within the weak-signal limit. After these considerations, we continue our discussion. We choose the size of the frequency bands $\Delta f = 1/T_{\rm obs}$. Hence, our covariance matrix becomes proportional to the identity

$$C_{IJ}^{-1} \approx \frac{2}{\sigma_p^4} \delta_{IJ}, \qquad (3.8)$$

and the log-likelihood reduces to a simple expression at a given frequency

$$\mathcal{L}_f = \frac{2}{(4\pi f \sigma_p^2)^2} \delta_{IJ} \mathcal{H}(\nu) \mathcal{I}(f/f_\star, c_0, z). \qquad (3.9)$$

The full likelihood requires a sum over all frequency bands: $\mathcal{L} = \sum_{{\rm band}(f)} \mathcal{L}_f$. We choose these bands ranging from $1/T_{\rm obs}$ to $20/T_{\rm obs}$. The Fisher matrix is obtained by computing second derivatives of the log-likelihood over the components θ_α of the vector $\vec{\theta}$ of parameters of interest and taking the expectation value

$$F_{\alpha\beta} = \left\langle \frac{\partial^2 \mathcal{L}}{\partial \theta_\alpha \partial \theta_\beta} \right\rangle. \qquad (3.10)$$

We restrict the vector of parameters to constrain to the quantities c_0 and z (recall that we are assuming that all sources are located at the same redshift). The Fisher matrix evaluates to

$$
\begin{aligned}
F_{\alpha\beta} &= \frac{1}{2} \sum_{{\rm band}(f/f_*)} {\rm Tr}(C_{IJ}^{-1} \partial_\alpha C_{IJ} C_{IJ}^{-1} \partial_\beta C_{IJ} + C_{IJ}^{-1}(\partial_\alpha \mu \partial_\beta \mu^T + \partial_\beta \mu \partial_\alpha \mu^T)), \\
&= \frac{1}{\sigma_p^4} \sum_{{\rm band}(f/f_*)} (\partial_\alpha \mu \partial_\beta \mu^T + \partial_\beta \mu \partial_\alpha \mu^T), \\
&= \frac{1}{(4\pi f)^2 \sigma_p^4} \sum_{{\rm band}(f/f_*)}
\begin{pmatrix}
2\frac{\partial \mathcal{R}_{ab}}{\partial c_0}\left(\frac{\partial \mathcal{R}_{ab}}{\partial c_0}\right)^T & \frac{\partial \mathcal{R}_{ab}}{\partial c_0}\left(\frac{\partial \mathcal{R}_{ab}}{\partial z}\right)^T + \frac{\partial \mathcal{R}_{ab}}{\partial z}\left(\frac{\partial \mathcal{R}_{ab}}{\partial c_0}\right)^T \\
\frac{\partial \mathcal{R}_{ab}}{\partial z}\left(\frac{\partial \mathcal{R}_{ab}}{\partial c_0}\right)^T + \frac{\partial \mathcal{R}_{ab}}{\partial c_0}\left(\frac{\partial \mathcal{R}_{ab}}{\partial z}\right)^T & 2\frac{\partial \mathcal{R}_{ab}}{\partial z}\left(\frac{\partial \mathcal{R}_{ab}}{\partial z}\right)^T
\end{pmatrix}.
\end{aligned} \qquad (3.11)
$$

The marginal error in the parameter θ_α we wish to constrain is given by

$$\Delta \theta_\alpha \geq \sqrt{(F)_{\alpha\alpha}^{-1}}. \qquad (3.12)$$

From these formulas, focusing on the quantity c_0 we wish to constrain [see Eq. (2.15)], we determine its error Δc_0, as a function of the number of pulsars $N_{\rm psr}$, marginalized over the redshift. We represent the result in the left panel of Fig. 3, plotting the relative error of the deviation $1 - c_0$ (again, marginalized over the redshift). For generating the plots in the Fisher analysis, we make use of the GETDIST package [65].

The plot exhibits a linear scaling of the error with the pulsar number $N_{\rm psr}$, such that a deviation of the order (for example) 10^{-1} may be discernible within a 10% relative error for $N_{\rm psr} \sim 1000$. We may consider this case more carefully and explore whether data, besides c_0, can also independently

---

[2]We note that the strength of the signal observed by various PTA collaborations means that currently PTAs operate in the intermediate, rather than the weak-signal regime. To keep our Fisher analysis simple, we have deliberately chosen noise parameters such that the weak-signal limit applies for our hypothetical future PTA. A more realistic analysis would use the lower noise levels of current PTAs or the expected noise levels of future PTAs and account for the full covariance matrix. Lowering the noise levels will lead to smaller error bars on the parameters of interest, but only up to a point. Once we reach the intermediate-/strong-signal limit, the signal variance takes over as the limiting factor in the measurement of the parameters of interest, preventing us from measuring these parameters with arbitrary precision.

constrain the common source redshift z (whose benchmark value is here $z = 1$). We represent error ellipses in the right panel of Fig. 3, showing that, in fact, we can obtain a good precision (of order 10%–20%) in the determination of z with c_0, if we monitor a sufficient number of pulsars. One may find that, for $\log_{10}(1 - c_0) = -1.3$, a 1-$\sigma$ result may be totally visible at $N_{\text{psr}} = 500$, and a 2-σ result may be visible for $N_{\text{psr}} = 2000$. Deviations from standard dispersion relations, then, can also be used as a ladder to determine the distance from the source. It would be interesting to further develop this topic, also studying possible ways to resolve degeneracies with $1 - c_0$ that are present in the right panel of Fig. 3. Intuitively, one possible source of degeneracy for this model may simply occur through the strength of the signal, with sources at lower z_0 increasing the magnitude of the bump characteristically associated with the strength of the deviation, c_0. Upon further analysis, this may be resolvable by closer inspection of the source distribution model over a variety of choices of z_0. We then choose to proceed along the lines of improving the source model in the proceeding section.

B. Refining the model: Integrating over redshift

In the analysis so far, we hypothesized that all sources appear at a common redshift. We now relax this assumption and work with the SMBH population model developed in [66], as used in [67]. See also [68] and references therein for a recent study with refinements on SMBH population scenarios. We already briefly commented around Eq. (2.14) about the mechanism by which our generalization of Phinney's theorem can accommodate integration over sources at distinct redshifts. The integration primarily depends on the dependence of the pulsar number over redshift. Distortions of the SGWB profile induced by modified dispersion relations can be used to probe the redshift dependence of the SMBH population. Concretely, we extend our previous analysis and wish to integrate the fitting formula (2.17) over redshift. We may then define

$$\Omega_{\text{GW}}(x, c_0, z) = \frac{1}{N_0} \int_0^z \tilde{\Omega}_{\text{GW}}(x, c_0, \tilde{z}) N(\tilde{z}) d\tilde{z}, \quad (3.13)$$

where $N(z)$ is the population at a given redshift, and $N_0 = \int dz N(z)$. The number density of sources emitting per redshift, per logarithmic chirp mass is obtained as

$$\frac{dn}{dz d\log_{10}\mathcal{M}} = \dot{n}_0 \left(\frac{\mathcal{M}}{10^7 \mathcal{M}_\odot}\right)^{-\alpha} e^{-\mathcal{M}/\mathcal{M}_*} (1 + z)^\beta e^{-z/z_0} \frac{dt_r}{dz}. \quad (3.14)$$

The quantity t_r represents the coordinate time in the source frame, and the parameters α and $\mathcal{M}_*$ govern the chirp mass distribution, while the parameters z_0 and β govern the redshift distribution (see Ref. [66] for more details). The normalized merger rate $\dot{n}_0$ is fixed such that the overall amplitude

TABLE I. The benchmark population model parameters we consider.

Model	α	$\mathcal{M}_*[\mathcal{M}_\odot]$	β	z_0
(1)	1	3.2×10^7	3	3
(2)	0.5	7.5×10^7	2.5	2.4
(3)	0	1.8×10^8	2	1.8

matches the profile in Eq. (3.1)—this may be fixed more rigorously with a treatment such as in [69], however, our simple fixing remains within the same bounds. One may then rewrite this in terms of the number of binaries in a spherical shell of thickness dz emitting at a frequency f_r such that

$$\frac{dn}{dz d\log_{10}\mathcal{M}} = \frac{dN}{dz d\log_{10}\mathcal{M} d\log_{10} f_r} \frac{d\log_{10} f_r}{dt_r} \frac{dt_r}{dz} \frac{dz}{dV_c}, \quad (3.15)$$

with V_c representing the comoving volume where

$$\frac{dt_r}{dz} \frac{dz}{dV_c} = \frac{1}{4\pi(1 + z)D_A^2}, \quad (3.16)$$

and D_A is the luminosity distance [1]. Further assuming the only change in f_r occurs due to energy loss from gravitational radiation yields

$$\frac{d\log_{10} f_r}{dt_r} = \frac{96}{5} \pi^{8/3} \mathcal{M}^{5/3} f_r^{8/3}. \quad (3.17)$$

Explicitly, we work with population models (1)–(3) examined in [67] (and originally in [66]). We report the benchmark values for the corresponding parameters in Table I. The population as a function of redshift is then

$$N(z) = \frac{5\dot{n}_0}{24\pi^{5/3}} \int \frac{1}{\mathcal{M}^{8/3}} \left(\frac{\mathcal{M}}{10^7 \mathcal{M}_\odot}\right)^{-\alpha} e^{-\frac{\mathcal{M}}{\mathcal{M}_*}} d\mathcal{M}$$
$$\times \int \frac{1}{f_r^{11/3}} df_r \int D_A^2 (1 + \tilde{z})^{\beta+1} e^{-\frac{\tilde{z}}{z_0}} d\tilde{z}. \quad (3.18)$$

Working such that $\mathcal{M} = 3.2 \times 10^7 \mathcal{M}_\odot$ appears as the upper limit of the integration over mass and again taking the reference frequency $f_* = 1 \times 10^{-8}$, we can numerically integrate to find a population structure shown in Fig. 4. This population model counts the number of contributing sources out to a given redshift $\tilde{z}$, whose contribution to the background is observed in Eq. (3.13). For this analysis, we assume $H_0 = 70 \text{ km s}^{-1} \text{ Mpc}^{-1}$, $\Omega_M = 0.3$, $\Omega_\Lambda = 0.7$, and $\Omega_k = 0$.

By performing the same kind of Fisher analysis as described in the previous subsection—always with the log-likelihood (3.10)—we can place constraints on the
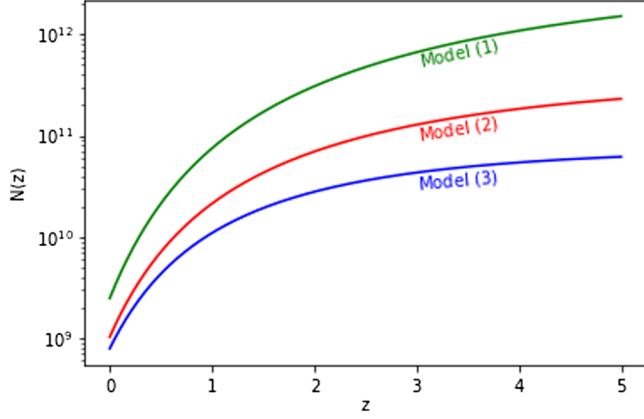
FIG. 4. The SMBH binary population models (1)–(3) of Table I, as a function of z for binaries with chirp mass $\mathcal{M} = 3.2 \times 10^7 \mathcal{M}_\odot$ emitting at the frequency f_*.

quantity c_0, by integrating sources up to a given redshift value. Figure 5 (and Table II) demonstrates the error bounds for c_0 for population model (1) (first row) and (3) (second row). Model (2) is an intermediate case among these (as can be guessed by Fig. 4) and we do not represent the results explicitly. We restrict the integration of sources up to $z = 1$ for both source population models, highlighting the increased precision of $1 - c_0$ for different values of monitored pulsar number N_{psr} and population model choices. Binaries at low redshift (or sources inducing large dispersion) will produce the dominant signal and amplify

the magnitude of the deviation due to modified gravity. This effect appears particularly prominent when comparing across population models—population model (1) reproduces a more homogeneous population of low-mass black hole binaries distributed relatively broadly across redshift. In comparison, population model (3) is more inhomogeneous and contains fewer, but more massive (and thus, louder) binaries distributed in a more concentrated nearby region. It would, therefore, be expected that this distribution provides a lower error in $1 - c_0$, as the signal sources will be more clearly resolved.

The results indicate that, within the hypothesis behind our analysis, values of $1 - c_0$ of order 10^{-2} can be tested around the level of 10% accuracy by monitoring many pulsars; however, the accuracy rapidly degrades as we reduce the values of $1 - c_0$. Including the population model appears to reduce the relative error by approximately 1 order of magnitude—which would be anticipated due to a more precise source-modeling scheme (as the results demonstrated in Fig. 5 are found by marginalizing over redshift, with the upper limit of the integration in z appearing as a Fisher parameter). We can interpret this upper limit as the redshift to the furthest source, and it characterizes the spread of the source distribution. For this model, we cannot take the redshift to be too large, as at large redshift, the fit model $\tilde{\Omega}_{\mathrm{GW}}$ begins to diverge. We also see from Table II that for population model (3), it may be possible to observe deviations on the order of $1 - c_0 = 10^{-3}$ with higher pulsar numbers. It would be very
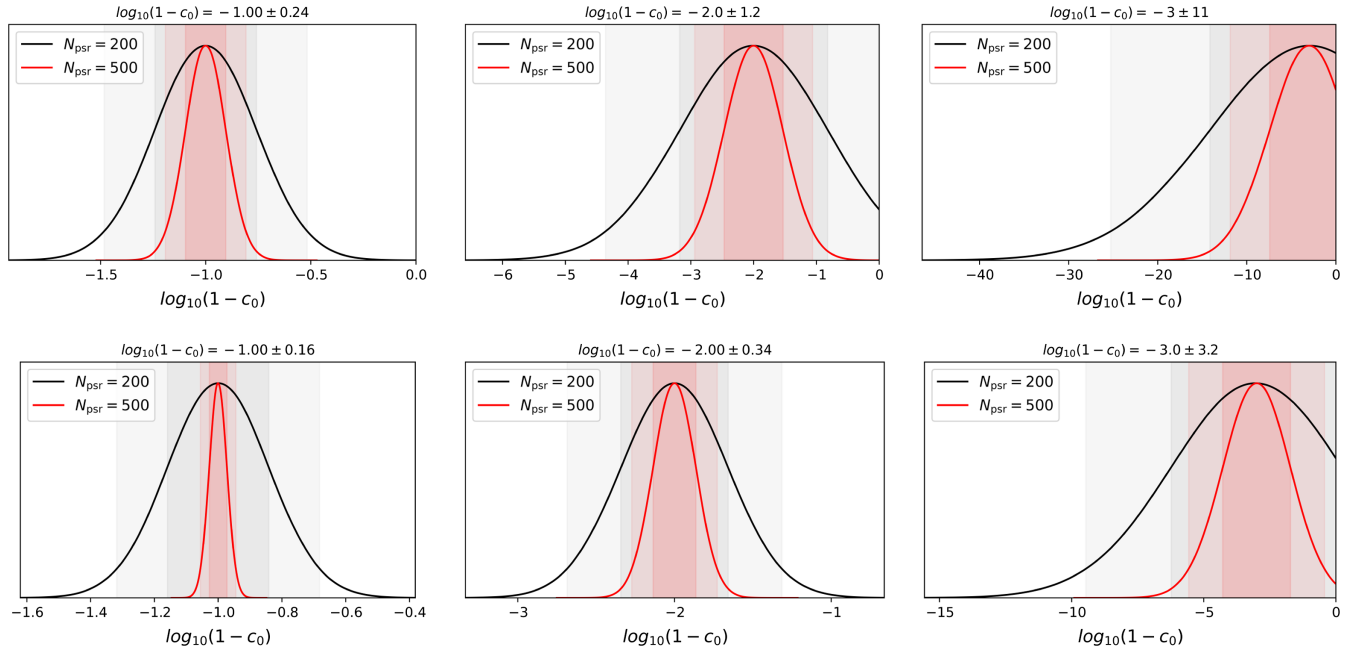

FIG. 5. The relative error bounds for $\log_{10}(1 - c_0) = -1, -2, -3$ benchmark values, integrating over redshift Eq. (3.18) to $z = 1$. First row: population model (1). Second row: population model (3). We select $N_{\mathrm{psr}} = 200$ and $N_{\mathrm{psr}} = 500$. In all plots, the darker bands represent a 1-σ deviation, and the lighter bands represent a 2-σ deviation. The quoted errors refer to the $N_{\mathrm{psr}} = 200$ case with all errors tabulated in Table II.

TABLE II. Tabulated results of Fig. 5 detailing the 1-σ resolution of each model, for $N_{psr} = 200, 500$.

$\log_{10}(1 - c_0)$	$\Delta \log_{10}(1 - c_0)$, $N_{psr} = 200$		$\Delta \log_{10}(1 - c_0)$, $N_{psr} = 500$	
	Model (1)	Model (3)	Model (1)	Model (3)
−1	0.24	0.16	0.10	0.03
−2	1.2	0.34	0.47	0.14
−3	11	3.2	4.43	1.28

interesting to refine our discussion and consider more realistic modeling for the pulsar noise or explore further source population models, for instance, (4) and (5) in [67] or phenomenological models as in [70], to discover their ability to constrain deviations from $c_0 = 1$, further pushing the boundaries of smaller detectable deviations.

IV. CONCLUSIONS

Several well-motivated scenarios of modified gravity, when applied to cosmological settings, predict that the speed of GWs is different from that of light. We generalized Phinney's practical theorem to scenarios with modified GW dispersion relations. The generalization is particularly interesting to consider in models predicting a frequency-dependent GW speed, which changes in a sizable way within the frequency band of a given detector. Adopting a well-motivated ansatz for modified GW dispersion relations, we pointed out that they can lead to a localized distortion on the SGWB frequency profile, potentially detectable by future experiments. We focused on the

SGWB produced in the initial inspiral phase by supermassive black hole binaries in circular orbits. By means of a dedicated Fisher analysis, we forecasted opportunities to detect modified gravity effects with PTA experiments, monitoring a large number of pulsars. We pointed out that these effects, in addition to modified gravity, also depend on the details of the source population, alongside redshift position of the GW sources. If detected, the effects we have highlighted can be used as cosmic ladders to infer cosmic distances. It would be interesting to further explore these ideas, which require careful discussion and analysis of intrinsic noise pulsar properties and further considerations of possible degeneracies with astrophysical effects. While we focused on applications to pulsar timing arrays working at nanohertz GW frequencies, our generalization of Phinney's theorem may readily be applied to other frequency bands and to ground- or space-based detectors; for example, to study possible modifications of the frequency profile of the SGWB caused by stellar origin binary black holes in the LISA band [71], which might be detected, for example, using the techniques proposed in [72]. We hope to return to investigate these possibilities in separate studies.

ACKNOWLEDGMENTS

DATA AVAILABILITY

No new data were generated for this manuscript.

[1] M. Maggiore, *Gravitational Waves. Vol. 1: Theory and Experiments* (Oxford University Press, Oxford, 2007).

[2] M. Maggiore, *Gravitational Waves. Vol. 2: Astrophysics and Cosmology* (Oxford University Press, Oxford, 2018).

[3] E. S. Phinney, A practical theorem on gravitational wave backgrounds, arXiv:astro-ph/0108028.

[4] B. P. Abbott *et al.* (LIGO Scientific and Virgo Collaborations), GW170817: Observation of gravitational waves from a binary neutron star inspiral, Phys. Rev. Lett. **119**, 161101 (2017).

[5] B. P. Abbott *et al.* (LIGO Scientific, Virgo, Fermi-GBM, and INTEGRAL Collaborations), Gravitational waves and gamma-rays from a binary neutron star merger: GW170817 and GRB 170817A, Astrophys. J. Lett. **848**, L13 (2017).

[6] B. P. Abbott *et al.* (LIGO Scientific, Virgo, Fermi GBM, INTEGRAL, IceCube, AstroSat Cadmium Zinc Telluride Imager Team, IPN, Insight-Hxmt, ANTARES, Swift, AGILE Team, 1M2H Team, Dark Energy Camera GW-EM, DES, DLT40, GRAWITA, Fermi-LAT, ATCA,

ASKAP, Las Cumbres Observatory Group, OzGrav, DWF (Deeper Wider Faster Program), AST3, CAASTRO, VINROUGE, MASTER, J-GEM, GROWTH, JAGWAR, CaltechNRAO, TTU-NRAO, NuSTAR, Pan-STARRS, MAXI Team, TZAC Consortium, KU, Nordic Optical Telescope, ePESSTO, GROND, Texas Tech University, SALT Group, TOROS, BOOTES, MWA, CALET, IKI-GW Follow-up, H.E.S.S., LOFAR, LWA, HAWC, Pierre Auger, ALMA, Euro VLBI Team, Pi of Sky, Chandra Team at McGill University, DFN, ATLAS Telescopes, High Time Resolution Universe Survey, RIMAS, RATIR, SKA South Africa/MeerKAT Collaborations), Multi-messenger observations of a binary neutron star merger, Astrophys. J. Lett. **848**, L12 (2017).

[7] P. Creminelli and F. Vernizzi, Dark energy after GW170817 and GRB170817A, Phys. Rev. Lett. **119**, 251302 (2017).

[8] J. Sakstein and B. Jain, Implications of the neutron star merger GW170817 for cosmological scalar-tensor theories, Phys. Rev. Lett. **119**, 251303 (2017).

[9] J. M. Ezquiaga and M. Zumalacárregui, Dark energy after GW170817: Dead ends and the road ahead, Phys. Rev. Lett. **119,** 251304 (2017).

[10] T. Baker, E. Bellini, P. G. Ferreira, M. Lagos, J. Noller, and I. Sawicki, Strong constraints on cosmological gravity from GW170817 and GRB 170817A, Phys. Rev. Lett. **119,** 251301 (2017).

[11] L. Lombriser and A. Taylor, Breaking a dark degeneracy with gravitational waves, J. Cosmol. Astropart. Phys. 03 (2016) 031.

[12] D. Bettoni, J. M. Ezquiaga, K. Hinterbichler, and M. Zumalacárregui, Speed of gravitational waves and the fate of scalar-tensor gravity, Phys. Rev. D **95,** 084029 (2017).

[13] I. D. Saltas, I. Sawicki, L. Amendola, and M. Kunz, Anisotropic stress as a signature of nonstandard propagation of gravitational waves, Phys. Rev. Lett. **113,** 191101 (2014).

[14] A. Nishizawa, Generalized framework for testing gravity with gravitational-wave propagation. I. Formulation, Phys. Rev. D **97,** 104037 (2018).

[15] A. Joyce, B. Jain, J. Khoury, and M. Trodden, Beyond the cosmological standard model, Phys. Rep. **568,** 1 (2015).

[16] G. Tasinato, Cosmic acceleration from Abelian symmetry breaking, J. High Energy Phys. 04 (2014) 067.

[17] D. Langlois and K. Noui, Degenerate higher derivative theories beyond Horndeski: Evading the Ostrogradski instability, J. Cosmol. Astropart. Phys. 02 (2016) 034.

[18] M. Crisostomi, K. Koyama, and G. Tasinato, Extended scalar-tensor theories of gravity, J. Cosmol. Astropart. Phys. 04 (2016) 044.

[19] J. Ben Achour, M. Crisostomi, K. Koyama, D. Langlois, K. Noui, and G. Tasinato, Degenerate higher order scalar-tensor theories beyond Horndeski up to cubic order, J. High Energy Phys. 12 (2016) 100.

[20] C. de Rham and S. Melville, Gravitational rainbows: LIGO and dark energy at its cutoff, Phys. Rev. Lett. **121,** 221101 (2018).

[21] C. de Rham and A. J. Tolley, Speed of gravity, Phys. Rev. D **101,** 063518 (2020).

[22] M. Bucher and D. N. Spergel, Is the dark matter a solid?, Phys. Rev. D **60,** 043505 (1999).

[23] J. Zaanen, F. Balm, and A. J. Beekman, Crystal gravity, SciPost Phys. **13,** 039 (2022).

[24] P. Szekeres, Linearized gravitation theory in macroscopic media, Ann. Phys. (N.Y.) **64,** 599 (1971).

[25] J. Madore, The dispersion of gravitational waves, Commun. Math. Phys. **27,** 291 (1972).

[26] J. Madore, The absorption of gravitational radiation by a dissipative fluid, Commun. Math. Phys. **30,** 335 (1973).

[27] W. H. Press, On gravitational conductors, waveguides, and circuits, Gen. Relativ. Gravit. **11,** 105 (1979).

[28] M. Raveri, C. Baccigalupi, A. Silvestri, and S.-Y. Zhou, Measuring the speed of cosmological gravitational waves, Phys. Rev. D **91,** 061501 (2015).

[29] J. Beltran Jimenez, F. Piazza, and H. Velten, Evading the Vainshtein mechanism with anomalous gravitational wave speed: Constraints on modified gravity from binary pulsars, Phys. Rev. Lett. **116,** 061101 (2016).

[30] T. Baker et al. (LISA Cosmology Working Group), Measuring the propagation speed of gravitational waves with LISA, J. Cosmol. Astropart. Phys. 08 (2022) 031.

[31] M. Colpi et al., LISA definition study report, arXiv:2402.07571.

[32] I. Harry and J. Noller, Probing the speed of gravity with LVK, LISA, and joint observations, Gen. Relativ. Gravit. **54,** 133 (2022).

[33] T. Baker, E. Barausse, A. Chen, C. de Rham, M. Pieroni, and G. Tasinato, Testing gravitational wave propagation with multiband detections, J. Cosmol. Astropart. Phys. 03 (2023) 044.

[34] S. S. Lahoz and J. Noller, Testing the speed of gravity with black hole ringdowns, Phys. Rev. D **107,** 124054 (2023).

[35] S. Mukohyama, E. Seraille, K. Takahashi, and V. Yingcharoenrat, Bridging dark energy and black holes with EFT: Frame transformation and gravitational wave speed, arXiv:2407.15123.

[36] G. Agazie et al. (NANOGrav Collaboration), The NANO-Grav 15 yr data set: Evidence for a gravitational-wave background, Astrophys. J. Lett. **951,** L8 (2023).

[37] D. J. Reardon et al., Search for an isotropic gravitational-wave background with the Parkes Pulsar Timing Array, Astrophys. J. Lett. **951,** L6 (2023).

[38] H. Xu et al., Searching for the nano-hertz stochastic gravitational wave background with the Chinese Pulsar Timing Array data release I, Res. Astron. Astrophys. **23,** 075024 (2023).

[39] J. Antoniadis et al. (EPTA and InPTA Collaborations), The second data release from the European Pulsar Timing Array—III. Search for gravitational wave signals, Astron. Astrophys. **678,** A50 (2023).

[40] A. Afzal et al. (NANOGrav Collaboration), The NANO-Grav 15 yr data set: Search for signals from new physics, Astrophys. J. Lett. **951,** L11 (2023).

[41] W. Qin, K. K. Boddy, and M. Kamionkowski, Subluminal stochastic gravitational waves in pulsar-timing arrays and astrometry, Phys. Rev. D **103,** 024045 (2021).

[42] Q. Liang, M.-X. Lin, and M. Trodden, A test of gravity with pulsar timing arrays, J. Cosmol. Astropart. Phys. 11 (2023) 042.

[43] N. Cordes, A. Mitridate, K. Schmitz, T. Schröder, and K. Wassner, On the overlap reduction function of pulsar timing array searches for gravitational waves in modified gravity, arXiv:2407.04464.

[44] G. Domènech and A. Tsabodimos, Finite distance effects on the Hellings-Downs curve in modified gravity, Eur. Phys. J. C **84,** 1005 (2024).

[45] E. Cannizzaro, G. Franciolini, and P. Pani, Novel tests of gravity using nano-hertz stochastic gravitational-wave background signals, J. Cosmol. Astropart. Phys. 04 (2024) 056.

[46] G. Ye and A. Silvestri, Can the gravitational wave background feel wiggles in spacetime?, Astrophys. J. Lett. **963,** L15 (2024).

[47] R. C. Bernardo and K.-W. Ng, Constraining gravitational wave propagation using pulsar timing array correlations, Phys. Rev. D **107,** L101502 (2023).

[48] G. Tasinato, Kinematic anisotropies and pulsar timing arrays, Phys. Rev. D **108,** 103521 (2023).

[49] R. C. Bernardo and K.-W. Ng, Beyond the Hellings-Downs curve: Non-Einsteinian gravitational waves in pulsar timing array correlations, Astron. Astrophys. **691,** A126 (2024).

[50] N. M. J. Cruz, A. Malhotra, G. Tasinato, and I. Zavala, Measuring the circular polarization of gravitational waves with pulsar timing arrays, Phys. Rev. D **110,** 103505 (2024).

[51] Y. Ali-Haïmoud, T. L. Smith, and C. M. F. Mingarelli, Fisher formalism for anisotropic gravitational-wave background searches with pulsar timing arrays, Phys. Rev. D **102,** 122005 (2020).

[52] Y. Ali-Haïmoud, T. L. Smith, and C. M. F. Mingarelli, Insights into searches for anisotropies in the nanohertz gravitational-wave background, Phys. Rev. D **103,** 042009 (2021).

[53] E. Belgacem, Y. Dirian, S. Foffa, and M. Maggiore, Gravitational-wave luminosity distance in modified gravity theories, Phys. Rev. D **97,** 104066 (2018).

[54] E. Belgacem, Y. Dirian, S. Foffa, and M. Maggiore, Modified gravitational-wave propagation and standard sirens, Phys. Rev. D **98,** 023510 (2018).

[55] Jose Maria Ezquiaga, Wayne Hu, Macarena Lagos, Meng-Xiang Lin, and Fei Xu, Modified gravitational wave propagation with higher modes and its degeneracies with lensing, J. Cosmol. Astropart. Phys. 08 (2022) 016.

[56] E. Belgacem *et al.* (LISA Cosmology Working Group), Testing modified gravity at cosmological distances with LISA standard sirens, J. Cosmol. Astropart. Phys. 07 (2019) 024.

[57] L. Z. Kelley, L. Blecha, and L. Hernquist, Massive black hole binary mergers in dynamical galactic environments, Mon. Not. R. Astron. Soc. **464,** 3131 (2017).

[58] G. Agazie *et al.* (NANOGrav Collaboration), The NANO-Grav 15 yr data set: Constraints on supermassive black hole binaries from the gravitational-wave background, Astrophys. J. Lett. **952,** L37 (2023).

[59] M. Tegmark, A. Taylor, and A. Heavens, Karhunen-Loeve eigenvalue problems in cosmology: How should we tackle large data sets?, Astrophys. J. **480,** 22 (1997).

[60] G. Janssen *et al.*, Gravitational wave astronomy with the SKA, Proc. Sci., AASKA14 (**2015**) 037.

[61] A. Weltman *et al.*, Fundamental physics with the square kilometre array, Pub. Astron. Soc. Aust. **37,** e002 (2020).

[62] R. W. Hellings and G. S. Downs, Upper limits on the isotropic gravitational radiation background from pulsar timing analysis, Astrophys. J. Lett. **265,** L39 (1983).

[63] J. Hazboun, J. Romano, and T. Smith, HASASIA: A PYTHON package for pulsar timing array sensitivity curves, J. Open Source Software **4,** 1775 (2019).

[64] N. M. J. Cruz, A. Malhotra, G. Tasinato, and I. Zavala, Measuring kinematic anisotropies with pulsar timing arrays, Phys. Rev. D **110,** 063526 (2024).

[65] A. Lewis, GETDIST: A PYTHON package for analysing Monte Carlo samples, arXiv:1910.13970.

[66] A. Sesana, A. Vecchio, and C. N. Colacino, The stochastic gravitational-wave background from massive black hole binary systems: Implications for observations with pulsar timing arrays, Mon. Not. R. Astron. Soc. **390,** 192 (2008).

[67] G. Sato-Polito and M. Kamionkowski, Exploring the spectrum of stochastic gravitational-wave anisotropies with pulsar timing arrays, Phys. Rev. D **109,** 123544 (2024).

[68] G. Sato-Polito and M. Zaldarriaga, The distribution of the gravitational-wave background from supermassive black holes, arXiv:2406.17010.

[69] S. Chen, A. Sesana, and C. J. Conselice, Constraining astrophysical observables of galaxy and supermassive black hole binary mergers using pulsar timing arrays, Mon. Not. R. Astron. Soc. **488,** 401 (2019).

[70] J. A. Casey-Clyde, C. M. F. Mingarelli, J. E. Greene, K. Pardo, M. Nañez, and A. D. Goulding, A quasar-based supermassive black hole binary population model: Implications for the gravitational wave background, Astrophys. J. **924,** 93 (2022).

[71] S. Babak, C. Caprini, D. G. Figueroa, N. Karnesis, P. Marcoccia, G. Nardini, M. Pieroni, A. Ricciardone, A. Sesana, and J. Torrado, Stochastic gravitational wave background from stellar origin binary black holes in LISA, J. Cosmol. Astropart. Phys. 08 (2023) 034.

[72] C. Caprini, D. G. Figueroa, R. Flauger, G. Nardini, M. Peloso, M. Pieroni, A. Ricciardone, and G. Tasinato, Reconstructing the spectral shape of a stochastic gravitational wave background with LISA, J. Cosmol. Astropart. Phys. 11 (2019) 017.